Research in Astron. Astrophys. **2013** Vol. **13** No. **1**, 47 – 56
http://www.raa-journal.org *http://www.iop.org/journals/raa*

***R**esearch in*
***A**stronomy and*
***A**strophysics*

Star formation associated with the infrared dust bubble N68

Chuan-Peng Zhang[1,2,3] and Jun-Jie Wang[1,2]

[1] National Astronomical Observatories, Chinese Academy of Sciences, Beijing 100012, China; *zcp0507@gmail.com*
[2] NAOC-TU Joint Center for Astrophysics, Lhasa 850000, China
[3] University of Chinese Academy of Sciences, Beijing 100049, China

Received 2012 June 27; accepted 2012 September 10

Abstract We investigated the environment of the infrared dust bubble N68 and searched for evidence of triggered star formation in its surroundings. We performed a multiwavelength study of the nebula with data taken from several large-scale surveys: GLIMPSE, MIPSGAL, IRAS, NVSS, GRS and JCMT. We analyzed the spectral profile and the distribution of the molecular gas (^{13}CO $J = 1 - 0$ and $J = 3 - 2$), and the dust in the environment of N68. The position-velocity diagram clearly shows that N68 may be expanding outward. We used two three-color images of the mid-infrared emission to explore the physical environment, and one color-color diagram to investigate the distribution of young stellar objects (YSOs). We found that the 24 μm emission is surrounded by the 8.0 μm emission. Morphologically, the 1.4 GHz continuum strongly correlates with the 24 μm emission, and the ^{13}CO $J = 1 - 0$ and $J = 3 - 2$ emissions correlate well with the 8.0 μm emission. We investigated two compact cores located in the shell of N68. The spectral intensity ratios of ^{13}CO $J = 3 - 2$ to $J = 1 - 0$ range from 5 to 0.3. In addition, YSOs, masers, IRAS and UC HII regions are distributed in the shell of the bubble. The active region may be triggered by the expansion of the bubble N68.

Key words: infrared: stars — stars: formation — ISM: bubbles — HII regions

1 INTRODUCTION

There are many signatures of star formation, for example, the presence of outflow/inflow, dark clouds and HII regions, which can be used to investigate the process of star formation. Also, there are many different kinds of interactions which can trigger star formation, such as a cloud-cloud collision (Li & Wang 2012), supernova explosion (Xu et al. 2011a,b), bubble expansion (Zhang & Wang 2012) and so on. Churchwell et al. (2006, 2007) detected and cataloged about 600 mid-infrared (MIR) dust bubbles between longitudes −60° and +60°. The bubbles have bright 8.0 μm shells that enclose bright 24 μm interiors. The infrared (IR) dust bubbles may be produced by exciting O- and/or B-type stars, which are located inside the bubble. The ultraviolet (UV) radiation from exciting stars may heat dust and ionize the gas to form an expanding bubble shell (Watson et al. 2008), which is known as the "collect-and-collapse" process. This process can trigger massive star formation near the shell clumps. Therefore, the bubbles present an important opportunity to study the interaction between the HII regions and molecular clouds.

A few individual bubbles have been thoroughly studied, such as N49 and S51. There are many models and observations to explain the dusty wind-blown bubbles, such as bubble N49 of Everett & Churchwell (2010). Recently, we reported an expanding bubble S51 shown with a shell and a front side, employing ^{13}CO and C^{18}O $J = 1 - 0$ emission lines (Zhang & Wang 2012). Beaumont & Williams (2010) reported CO $J = 3-2$ maps of 43 bubbles identified by Spitzer. Watson et al. (2008) present an analysis of wind-blown, parsec-sized, MIR bubbles and their associated star formation.

To increase the number of examples of bubbles that have been investigated, we selected the IR dust bubble [CPA2006] N68 (hereafter N68) from the catalog of Churchwell et al. (2006). N68 is complete or closed ring and centered on Galactic coordinates $l = 35.654$, $b = -0.062$ (or R.A.(J2000) = $18^{h}56^{m}25^{s}.70$, Dec.(J2000) = $02^{\circ}26'01''.0$). It has a distance of 10.6 kpc, which was obtained by Anderson & Bania (2009) based on comparing the velocity of the ionized gas with the maximum velocity of HI absorption, and looking for HI absorption at the velocity of molecular emission. In addition, its size is 34 pc $\times$ 17 pc and the eccentricity of the ellipse is 0.72.

In this work, we mainly present a multiwavelength study of the environment surrounding the IR dust bubble N68. We explore its surrounding interstellar medium (ISM) and search for signatures of star formation. The observations and data are described in Section 2; the results and discussions about the environment of bubble N68 are presented in Section 3; Section 4 summarizes the results.

2 DATA

We analyzed IR and millimeter wavelength data extracted from several large-scale surveys including GLIMPSE (Benjamin et al. 2003; Churchwell et al. 2009), MIPSGAL (Carey et al. 2009), IRAS (Neugebauer et al. 1984), NVSS (Condon et al. 1998), GRS[1] and JCMT[2].

GLIMPSE is an MIR survey of the inner Galaxy performed with the Spitzer Space Telescope. We used the mosaicked images from the GLIMPSE and the GLIMPSE Point-Source Catalog (GPSC) in the Spitzer-IRAC (3.6, 4.5, 5.8 and 8.0 μm). IRAC has an angular resolution of between 1.5″ and 1.9″ (Fazio et al. 2004; Werner et al. 2004). MIPSGAL is a survey of the same region as GLIMPSE, using the MIPS instrument on Spitzer. The MIPSGAL resolution is 6″ at 24 μm. The 60 and 100 μm fluxes of the IRAS were employed to estimate the Lyman continuum ionizing flux. The NRAO VLA Sky Survey (NVSS) is a 1.4 GHz continuum survey covering the entire sky north of -40° declination (Condon et al. 1998).

The 14-m GRS has a full width at half maximum (FWHM) beam size of $\sim$ 46″ at $\sim$110 GHz for ^{13}CO $J = 1 - 0$ transitions. Each field of the GRS in the ^{13}CO $J = 1 - 0$ line comprises spectra on a fully sampled 22″ grid. The intensities are on a $T_{\rm A}^{*}$ antenna temperature scale. To convert this to main beam temperature, $T_{\rm A}^{*}$ is divided by the main beam efficiency of 0.48. The velocity resolution of the data is 0.25 km s^{-1} (0.22 km s^{-1} sampling) (Jackson et al. 2006). The 15-m JCMT has an FWHM beam size of $\sim$ 14″ at $\sim$330 GHz for ^{13}CO $J = 3 - 2$ transitions. The correlator was configured with 4096 channels over a 250-MHz bandwidth, which provided a velocity resolution of $\sim$0.055 km s^{-1} per channel. The spectra of ^{13}CO $J = 1-0$ and $J = 3-2$ have been smoothed to a velocity resolution of 0.50 and 0.44 km s^{-1}, respectively.

The ^{13}CO $J = 1 - 0$ and the ^{13}CO $J = 3 - 2$ data cubes were processed with CLASS and GREG in the GILDAS software package[3].

[1] This publication makes use of molecular line data from the Boston University- FCRAO Galactic Ring Survey (GRS). The GRS is a joint project between Boston University and the Five College Radio Astronomy Observatory (FCRAO), funded by the National Science Foundation under grants AST-9800334, AST-0098562, AST-0100793, AST-0228993 & AST-0507657.

[2] The James Clerk Maxwell Telescope is operated by the Joint Astronomy Centre on behalf of the Science and Technology Facilities Council of the United Kingdom, the Netherlands Organisation for Scientific Research and the National Research Council of Canada.

[3] *http://iram.fr/IRAMFR/GILDAS/*

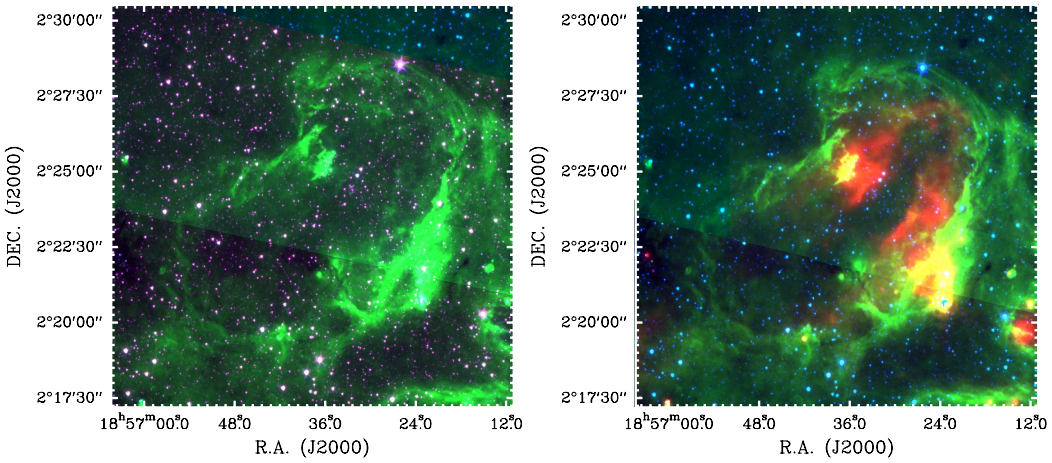

Fig. 1 Mid-IR emission of the IR dust bubble N68. *Left*: Spitzer-IRAC three-color image (3.6 μm = red, 4.5 μm = blue and 8.0 μm = green); *Right*: Spitzer-IRAC and Spitzer-MIPSGAL three-color image (4.5 μm = blue, 8.0 μm = green and 24 μm = red).

3 RESULTS AND DISCUSSIONS

3.1 The IR Dust Distribution of N68

Two Spitzer three-color images of N68 are shown in Figure 1. Both figures clearly illustrate the photo-dissociation region (PDR) visible in 8.0 μm (in green) emission, which originates mainly in the polycyclic aromatic hydrocarbons (PAHs). As these large molecules inside the ionized region are destroyed, the PAH emission delineates the boundaries of the HII region, and molecular clouds inside are excited in the PDR by the radiation leaking from the HII region (Petriella et al. 2010; Pomarès et al. 2009). The 24 μm emission (right panel in Fig. 1), appearing just in the northwest part of bubble N68, corresponds to hot dust. It is likely that O- and/or early B-type stars produced the bubble shell of this HII region, with hot dust located inside the bubble. The 3.6 μm emission (in red, left panel in Fig. 1) shows the positions of different stars.

In addition, the molecular gas of the bubble shell exhibits several clumps and filaments along the PDR shell seen from Figure 1. The distribution and morphology of this material suggests that a collect-and-collapse process may be occurring.

3.2 The Continuum Emission and Clump Structure

The entire bubble N68 fills the 1.4 GHz continuum from NVSS (left panel in Fig. 2), which is particularly saturated in the northwest part. This area, saturated with emission detected by the NVSS, morphologically correlates with the 24 μm emission in Figure 1. We suggest that exciting stars, which are radiating strong UV radiation, may exist in this region. Possibly because of the obstruction from the molecular cloud, the hot dust develops and permeates into the southeast part of N68.

The ^{13}CO $J = 3 - 2$ contours (Figure 2 right panel) from the JCMT data show several clumps, which may be the birthplace of young stellar objects (YSOs). In Table 1, we list the coordinates of several YSO candidates, which are indicated with symbols "▲," "■," and "★" in Figure 2. These contours are distributed over almost the entire 8.0 μm shell of the bubble. Southwest of N68, there are two strong cores which will be investigated in Section 3.4.

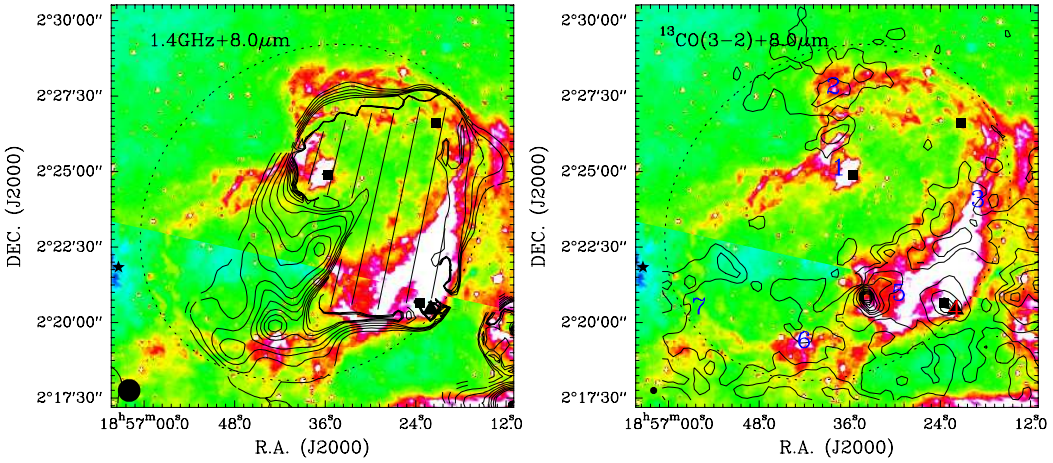

Fig. 2 Integrated velocity contours of 1.4 GHz continuum (*Left panel*) and ^{13}CO $J = 3 - 2$ (*Right panel*), superimposed on the GLIMPSE 8.0 μm color images. The contour levels are from 0.16 to 1.45 in steps of 0.16 mJy beam^{-1} for the 1.4 GHz continuum, while the contour levels are from 6.08, 12.17 to 121.70 in steps of 12.17 K km s^{-1} for ^{13}CO $J = 3 - 2$. The integrated velocity range is from 38.5 to 68.8 km s^{-1} for ^{13}CO $J = 3 - 2$. The symbols "▲," "■," and "★" indicate the positions of the maser (H_2O and OH), the IRAS point source and the EGO source, respectively. The beam size is shown by a black filled circle. Note that the 1.4 GHz continuum is saturated with oblique lines in the image.

Table 1 YSOs around Bubble N68

Source	Name	R.A. (J2000) (h m s)	Dec. (J2000) (° ′ ″)
IRAS	IRAS18538+0222	18 56 21.30	+02 26 37.00
IRAS	IRAS18538+0216	18 56 23.50	+02 20 38.00
IRAS	IRAS18540+0220	18 56 35.60	+02 24 54.00
CHII	G35.590-0.025	18 56 22.67	+02 21 14.58
EGO	G35.040-0.470	18 57 03.30	+02 21 50.00
Maser	G35.578-0.031	18 56 22.55	+02 20 28.10
UCHII	G35.578-0.031	18 56 22.64	+02 20 26.30

The 1.4 GHz continuum flux is about 1.27 Jy within this bubble. The number of stellar Lyman photons, absorbed by the gas in the HII region, follows the relationship (Mezger et al. 1974)

$$\left[\frac{N_{LyC}}{\mathrm{s}^{-1}}\right] = 4.761 \times 10^{48} \cdot a(\nu, T_\mathrm{e})^{-1} \cdot \left[\frac{\nu}{\mathrm{GHz}}\right]^{0.1} \cdot \left[\frac{T_\mathrm{e}}{\mathrm{K}}\right]^{-0.45} \cdot \left[\frac{S_\nu}{\mathrm{Jy}}\right] \cdot \left[\frac{D}{\mathrm{kpc}}\right]^2, \quad (1)$$

where $a(\nu, T_\mathrm{e})$ is a slowly varying function tabulated by Mezger & Henderson (1967); for the effective temperature of an exciting star $T_\mathrm{e} \sim 33\,000$ K and at radio wavelengths, $a(\nu, T_\mathrm{e}) \sim 1$. Finally, we obtain the flux of Lyman continuum ionizing photons as being $\log N_\mathrm{L} \sim 48.79$. Assuming the exciting stars belong to an O9.5 star with $\log N_\mathrm{L} = \sim 47.84$ (Panagia 1973), we suggest there should be about 8.89 exciting stars that ionize the bubble. There are presumably many other non-IR excess sources within the bubble that could also be O- and/or early B-type stars.

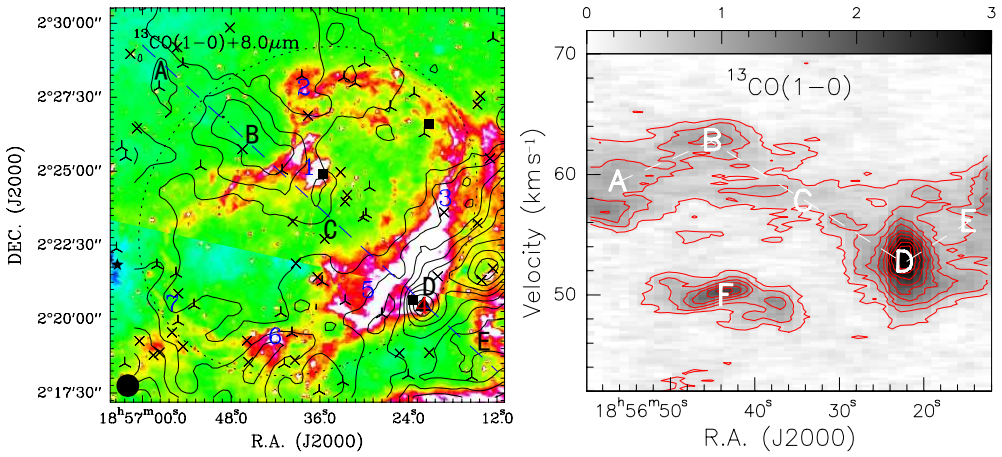

Fig. 3 *Left*: integrated velocity contours of the ^{13}CO $J = 1 - 0$ emission superimposed on the GLIMPSE 8.0 μm color image. The contour levels are from 14.23 to 61.66 in steps of 4.74 K km s^{-1}, and the integrated velocity range is from 38.5 to 68.8 km s^{-1}. The dotted ellipse shows the PAH morphology of the bubble. These numbers give the chosen positions of seven sources. The YSO candidates of class I and II are indicated with symbols "×," and "⅄" respectively. The symbols "▲," "■," and "★" indicate the positions of the maser (H_2O and OH), the IRAS point source and the EGO source, respectively. The beam size is shown by a black filled circle. *Right*: the position-velocity diagram of the ^{13}CO $J = 1 - 0$ emission along the dashed line in the left panel. The contour levels are from 0.35 to 3.18 in steps of 0.36 K.

3.3 The Distributions of the ^{13}CO $J = 1 - 0$ Molecular Clouds

3.3.1 Opacity, column density, and mass

We used ^{13}CO $J = 1 - 0$ to derive the opacity, column density, and mass of the nebula within the plot shown in Figure 3. The size of the plot is 13.3′×13.3′. The velocity range is from ∼38.5 to ∼68.8 km s^{-1}. The plot is centered on R.A.(J2000) = 18^{h}56^{m}25^s.70, Dec.(J2000) = 02°26′01″.0.

Here we assume that the nebula is in local thermodynamic equilibrium (LTE). We used the theory of radiation transfer and molecular excitation (Winnewisser et al. 1979; Garden et al. 1991). The ^{13}CO $J = 1 - 0$ opacity is gained from the equation

$$\tau(^{13}\mathrm{CO}) = -\ln\left[1 - \frac{T_{\mathrm{MB}}(^{13}\mathrm{CO})}{5.3}\left\{\left[\exp\left(\frac{5.3}{T_{\mathrm{ex}}} - 1\right)\right]^{-1} - 0.16\right\}^{-1}\right], \quad (2)$$

where T_{ex} is excitation temperature. The ^{13}CO $J = 1-0$ column density is obtained from the equation

$$N(^{13}\mathrm{CO}) = 2.4 \times 10^{14} \cdot \frac{T_{\mathrm{ex}} \int \tau(^{13}\mathrm{CO}) dv}{1 - \exp(-5.29/T_{\mathrm{ex}})}. \quad (3)$$

We assume that ^{13}CO $J = 1 - 0$ is optically thin, the excitation temperature is $T_{\mathrm{ex}} = 20$ K and the [H_2/^{13}CO] abundance ratio is 7×10^5 (Frerking et al. 1982). The molecular hydrogen column density $N(H_2)$ was then calculated. The molecular cloud mass is estimated at $M_{\mathrm{N68}} \sim 4.6 \times 10^5 M_\odot$ including the entire shell of bubble N68 at a distance of $D_{\mathrm{N68}} \sim 10.6$ kpc.

3.3.2 Clump structure

Figure 3 shows the integrated velocity contours of the ^{13}CO $J = 1 - 0$ emission superimposed on the GLIMPSE 8.0 μm color image. The integrated velocity range is from 38.5 to 68.8 km s^{-1}. Generally, there should be a similar sketch between the distributions of the millimeter emission and Mid-IR emission (Petriella et al. 2010; Zhang et al. 2012). Comparing the morphologic distribution (Fig. 3), there are many correlations between the contours and the 8.0 μm emission, however, their peak positions deviate slightly from each other. In addition, the nebula is clumped and extends outside the bubble. Therefore we have selected seven sources (1 ~ 7; indicated in Fig. 3) to investigate their spectral information in Section 3.3.4.

Along the dashed line in the left panel of Figure 3, we show the position-velocity diagram in the right panel. Figure 3 shows that the components of sources A, B, C, D and E are correlated with N68, but the component of source F is not. The components of sources A, B, C, D and E are made up of a morphology in the shape of a letter "*N*" in the position-velocity diagram (right panel of Fig. 3). Source C inside bubble N68 has only one velocity component. From source B (in the shell of the bubble) to source D (in the shell of the bubble), the position-velocity diagram does not show the shape of a letter "*U*." This is not consistent with the model of an expanding bubble inside a turbulent medium (Arce et al. 2011). However, considering the eccentricity of the bubble and positions of sources A, B, C, D and E, we also suggest that bubble N68 may be expanding toward the outside. The systematic velocity of N68 is ~58 km s^{-1} (the source C inside the bubble), and the velocities are ~59 and ~57 km s^{-1} for sources A and B outside the bubble, respectively. Also, the velocities are ~63 and ~53 km s^{-1} for sources B and D in the shell of the bubble. So bubble N68 may be expanding with a velocity of ~5 km s^{-1} along the line of sight relative to source C.

3.3.3 Distribution of the young stars

The color-color diagram (Fig. 4) shows the distribution of class I, II and III stars. Here we only consider those sources that have been detected in four Spitzer-IRAC bands (Hora et al. 2008). In addition, to look for a relationship between the young stars and the bubble formation, we draw the class I and II stars on the image of 8.0 μm emission for N68 (Fig. 3). We found that class I and II stars are almost all distributed on the shell of the bubble. The distribution of class I and II stars is also correlated with the ^{13}CO cloud. We also report the distributions of the IRAS data, the extended green object (EGO), the maser and the UC HII region, whose coordinates are listed in Table 1. These star formation tracers are located near and on the shell of the nebula. It is possible that the shell of the bubble is the birthplace of young stars, which could be the result of an interaction between the HII region and molecular cloud. This could be an example of the collect-and-collapse process.

3.3.4 The spectra of the ^{13}CO $J = 1 - 0$ *and* $J = 3 - 2$

Figure 5 shows the ^{13}CO $J = 1 - 0$ and $J = 3 - 2$ spectra of sources 1, 2, 3, 4, 5, 6 and 7 on the shell of the nebula. The average of all spectra from the whole bubble is exhibited (indicated with *All*) in the upper-left panel of Figure 5. This shows that the spectra of ^{13}CO $J = 1 - 0$ have a wider width and stronger intensity than those of $J = 3 - 2$. At sources 2 and 5, however, the spectra of ^{13}CO $J = 3 - 2$ have a stronger intensity than those of $J = 1 - 0$. The ^{13}CO $J = 1 - 0$ spectrum of source 4 does not have the ~61 km s^{-1} component relative to $J = 3 - 2$. In addition, from the contours, the ^{13}CO $J = 3 - 2$ distribution (Fig. 3) is clumpier than that of $J = 1 - 0$ (Fig. 2). Therefore, there is a great difference between ^{13}CO $J = 1 - 0$ and $J = 3 - 2$, which needs further investigation.

The intensity ratio of ^{13}CO $J = 3 - 2$ to $J = 1 - 0$ is $R^{13}_{3-2/1-0} = 0.46$, 3.53, 0.38, 0.70, 2.69 and 0.46 for sources *All*, 2, 3, 4, 5 and 6, respectively. Our results are consistent with those of Minamidani et al. (2011), whose $R^{13}_{3-2/1-0}$ ranges from 3.6±0.9 to 0.24±0.07. This suggests that ^{13}CO $J = 1 - 0$

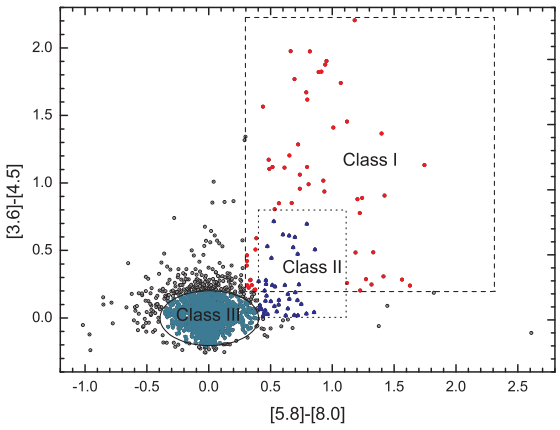

Fig. 4 The color-color diagram between [5.8–8.0] and [3.6–4.5] of the GLIMPSE data. Class I, II and III stars at different evolutionary stages are indicated in the diagram.

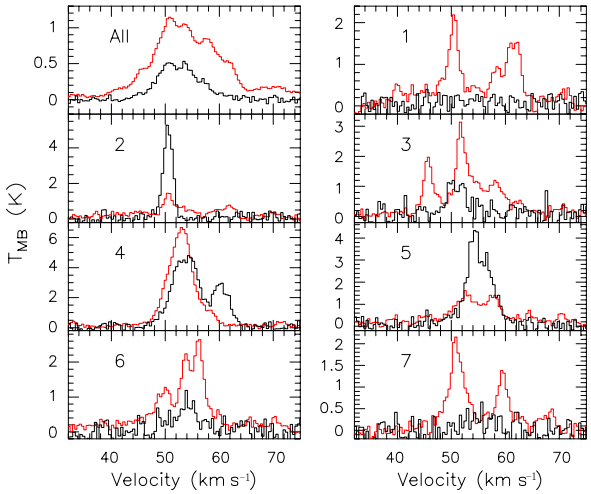

Fig. 5 ^{13}CO $J = 1 - 0$ (*red line*) and $J = 3 - 2$ (*gray line*) spectra of sources 1 to 7, whose positions are represented in Fig. 3 with numbers 1 to 7 respectively. All indicates that the two spectra are the spectral average of bubble N68.

and $J = 3-2$ transitions have different critical densities, so $R^{13}_{3-2/1-0}$ traces the excitation of molecular gas.

3.4 Two Compact Cores in the Shell of N68

There are two compact cores, M (R.A.(J2000) = $18^h56^m33^s.73$, Dec.(J2000) = $2°20'49''.81$) and N (R.A.(J2000) = $18^h56^m23^s.07$, Dec.(J2000) = $2°20'33''.44$), located in the southwest shell of N68.

Figure 6 shows the integrated velocity contours of the ^{13}CO $J = 1 - 0$ and $J = 3 - 2$ emission. The cores M and N are located at the peaks of integrated velocity contours of the ^{13}CO $J = 3 - 2$

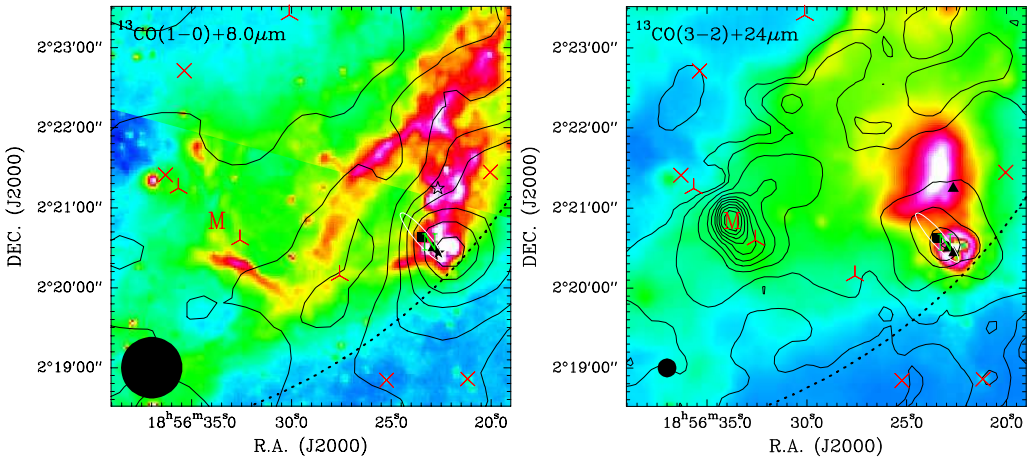

Fig. 6 Integrated velocity contours of the ^{13}CO $J = 1 - 0$ and $J = 3 - 2$ emission superimposed on the GLIMPSE 8.0 and 24 μm color images, respectively. The contour levels are from 14.23 to 61.66 in steps of 4.74 K km s^{-1} for ^{13}CO $J = 1 - 0$, and from 6.65, 13.30 to 119.68 in steps of 13.29 K km s^{-1} for ^{13}CO $J = 3 - 2$; the integrated velocity range is from 38.5 to 68.8 km s^{-1}. The dotted ellipse shows the PAH morphology of the bubble. These numbers give the chosen positions of three sources. The YSO candidates of class I and II are indicated with symbols "×" and "⅄." The symbols "▲" and "■," unfilled star and "★" indicate the positions of the maser (H_2O and OH), the IRAS point source, the compact HII region and the UC HII region, respectively. The white ellipse indicates the error ellipse of the IRAS point source.

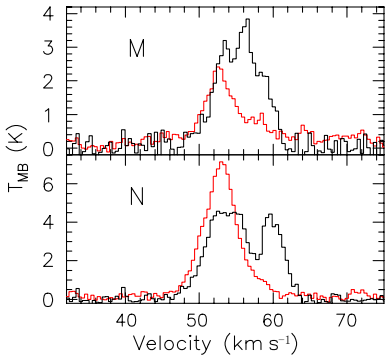

Fig. 7 ^{13}CO $J = 1 - 0$ (red line) and $J = 3 - 2$ (gray line) spectra of compact cores M (R.A.(J2000) = 18^{h}56^{m}33^{s}.73, Dec.(J2000) = 2°20′49″.81) and N (R.A.(J2000) = 18^{h}56^{m}23^{s}.07, Dec.(J2000) = 2°20′33″.44), whose positions are also represented in Fig. 6.

emission. The peak of the contours for ^{13}CO $J = 1 - 0$ is located at core N, but such a peak does not appear for core M. In addition, the difference between the 8.0 and 24 μm emission is obvious. The presence of the 24 μm emission is suggestive that the hot dust has plunged into the bubble shell.

On the other hand, there are many star formation tracers located near core N. In Figure 6, we marked the positions of an H_2O maser, an OH maser, an IRAS point source, a compact HII region, and a UC HII region, whose coordinates are listed in Table 1. The H_2O maser, the OH maser, the

IRAS point source and the UC HII region are located at the core N. There are many velocity components for the H_2O maser and the OH maser. We just list three of their strongest components. The fluxes are 20.15 Jy at 48.90 km s^{-1}, 7.25 Jy at 49.45 km s^{-1} and 2.80 Jy at 48.35 km s^{-1} for H_2O maser emission, but 9.90 Jy at 50.00 km s^{-1}, 4.40 Jy at 46.05 km s^{-1} and 3.70 Jy at 47.36 km s^{-1} for the OH maser emission (Forster & Caswell 1999). These are suggestive that core N is a strongly active massive star forming region.

We also exhibit the spectra of cores M and N in Figure 7. The difference in spectral profiles between emissions from ^{13}CO $J = 1 - 0$ and $J = 3 - 2$ is obvious. The ^{13}CO $J = 3 - 2$ has double profiles for cores M and N, but the ^{13}CO $J = 1 - 0$ lacks the blue profile. For core N, the ^{13}CO $J = 1 - 0$ has a main beam temperature of ∼7 K at ∼53 km s^{-1}, but the ^{13}CO $J = 3 - 2$ shows a flat spectrum of absorption. This discrepancy needs to be investigated further.

4 CONCLUSIONS

We have investigated the environment of the IR dust bubble N68 with the ^{13}CO $J = 1 - 0$ and $J = 3 - 2$ emission lines, the 1.4 GHz continuum and the IR band emission. The main results can be summarized as follows.

The morphology of the molecular line emission (^{13}CO $J = 1 - 0$ and $J = 3 - 2$) and the associated velocity signatures are consistent with the shell structure seen from the 8.0 μm images. The expanding shells in N68 are suggestive of triggered massive star formation. There is evidence for dense clumps that coincide with the shells. The expanding shells have an expansion speed of ∼5 km s^{-1}. However, it is not clear whether the HII region is the driving mechanism of the shell expansion.

We have presented a study about compact cores M and N located in the shell of the nebula. Compact core N is associated with the H_2O maser, the OH maser, the IRAS point source and the UC HII region. The spectral velocity components of the H_2O maser and the OH maser indicate that the star formation region is strongly active. However, properties of the processes occurring in the compact cores M and N need further investigation.

We also used the GLIMPSE and the MIPSGAL survey data to analyze the YSOs and the distribution of warm dust around bubble N68. We identified class I and II YSOs using the [5.8]–[8.0] versus [3.6]–[4.5] relationship, and correlated their distribution relative to the PDR, which we assume to be associated with and surrounding an HII region. We find that N68 appears to have a significant number of YSOs associated with their PDRs, implying that triggered star formation mechanisms act on the boundary of the expanding HII region.

Acknowledgements This work was supported by the Young Researcher Grant of the National Astronomical Observatories, Chinese Academy of Sciences (Grant No. O835032002).

References

Anderson, L. D., & Bania, T. M. 2009, ApJ, 690, 706
Arce, H. G., Borkin, M. A., Goodman, A. A., Pineda, J. E., & Beaumont, C. N. 2011, ApJ, 742, 105
Beaumont, C. N., & Williams, J. P. 2010, ApJ, 709, 791
Benjamin, R. A., Churchwell, E., Babler, B. L., et al. 2003, PASP, 115, 953
Carey, S. J., Noriega-Crespo, A., Mizuno, D. R., et al. 2009, PASP, 121, 76
Churchwell, E., Babler, B. L., Meade, M. R., et al. 2009, PASP, 121, 213
Churchwell, E., Povich, M. S., Allen, D., et al. 2006, ApJ, 649, 759
Churchwell, E., Watson, D. F., Povich, M. S., et al. 2007, ApJ, 670, 428
Condon, J. J., Cotton, W. D., Greisen, E. W., et al. 1998, AJ, 115, 1693
Everett, J. E., & Churchwell, E. 2010, ApJ, 713, 592

Fazio, G. G., Hora, J. L., Allen, L. E., et al. 2004, ApJS, 154, 10
Forster, J. R., & Caswell, J. L. 1999, A&AS, 137, 43
Frerking, M. A., Langer, W. D., & Wilson, R. W. 1982, ApJ, 262, 590
Garden, R. P., Hayashi, M., Hasegawa, T., Gatley, I., & Kaifu, N. 1991, ApJ, 374, 540
Hora, J. L., Carey, S., Surace, J., et al. 2008, PASP, 120, 1233
Jackson, J. M., Rathborne, J. M., Shah, R. Y., et al. 2006, ApJS, 163, 145
Li, N., & Wang, J.-J. 2012, RAA (Research in Astronomy and Astrophysics), 12, 1269
Mezger, P. G., & Henderson, A. P. 1967, ApJ, 147, 471
Mezger, P. G., Smith, L. F., & Churchwell, E. 1974, A&A, 32, 269
Minamidani, T., Tanaka, T., Mizuno, Y., et al. 2011, AJ, 141, 73
Neugebauer, G., Habing, H. J., van Duinen, R., et al. 1984, ApJ, 278, L1
Panagia, N. 1973, AJ, 78, 929
Petriella, A., Paron, S., & Giacani, E. 2010, A&A, 513, A44
Pomarès, M., Zavagno, A., Deharveng, L., et al. 2009, A&A, 494, 987
Watson, C., Povich, M. S., Churchwell, E. B., et al. 2008, ApJ, 681, 1341
Werner, M. W., Roellig, T. L., Low, F. J., et al. 2004, ApJS, 154, 1
Winnewisser, G., Churchwell, E., & Walmsley, C. M. 1979, A&A, 72, 215
Xu, J.-L., Wang, J.-J., & Miller, M. 2011a, ApJ, 727, 81
Xu, J.-L., Wang, J.-J., & Miller, M. 2011b, RAA (Research in Astronomy and Astrophysics), 11, 537
Zhang, C. P., Esimbek, J., Zhou, J. J., Wu, G., & Du, Z. M. 2012, Ap&SS, 337, 283
Zhang, C. P., & Wang, J. J. 2012, A&A, 544, A11